

# Determining the high-pressure phase transition in highly-ordered pyrolytic graphite with time-dependent electrical resistance measurements

Jeffrey M. Montgomery,<sup>1,2,a)</sup> Boris Kiefer,<sup>1</sup> and Kanani K. M. Lee<sup>1,3,b)</sup>

<sup>1</sup>*Department of Physics, New Mexico State University, MSC 3D, P.O. Box 30001, Las Cruces, New Mexico 88003-8001, USA*

<sup>2</sup>*Department of Physics, University of Alabama at Birmingham, 1530 3rd Ave. S, CH310, Birmingham, Alabama 35294-1170, USA*

<sup>3</sup>*Department of Geology and Geophysics, Yale University, 210 Whitney Ave., New Haven, Connecticut 06511, USA*

(Received 25 April 2011; accepted 21 July 2011; published online 31 August 2011)

Long-duration, high-pressure resistance measurements on highly-ordered pyrolytic graphite in a diamond-anvil cell show a sluggish phase transition occurring at  $\sim 19$  GPa, as evidenced by the time-dependent behavior of the sample resistance. The instantaneous resistance response to pressure adjustment shows a  $\sim 10$  GPa hysteresis that has been observed previously, rendering the conjectured direct relationship between resistance and phase-transition tentative. In contrast, the evolution of the resistance with time after the instantaneous response shows a systematic, reproducible, and distinct behavior, which allows reducing the uncertainty in transition pressure to  $\sim 2$  GPa. This largely reduced hysteresis shows explicitly that the phase transition is directly related to changes in electronic structure and resistance and establishes consistency with other commonly used experimental techniques to explore phase transitions at high pressures. We augment our experiments with first-principle density-functional theory computations to evaluate the pressure dependence of the electronic density of states of proposed candidate structures for the post-graphite phase. © 2011 American Institute of Physics. [doi:10.1063/1.3627372]

## I. INTRODUCTION

It has long been known that graphite exhibits a room-temperature phase transition between 10 and 20 GPa.<sup>1</sup> This transition was first observed by measuring the change in the electrical resistance along the *c*-axis of a graphite sample compressed along the *a*-axis in a standard Drickamer-type press,<sup>1</sup> and it was noted that the resistance exhibited a large ( $\sim 10$  GPa) hysteresis. Since then, several experiments<sup>2-5</sup> have confirmed the transition and the large magnitude of hysteresis in resistance. One challenge is to devise an experimental observable that pins down the transition pressure sufficiently to correlate electronic changes and structural transformations directly. Yet over the past five decades, no such observable has been devised, and no consensus on the transition pressure or on the structure of the resulting crystal-line phase has been reached. The lack of a coherent model for this transition in elemental carbon may be attributed to the different sensitivities of structural and electronic probes. The transition pressure may depend on the nature of the sample studied<sup>6</sup>: later studies on high purity<sup>7</sup> and well-ordered samples<sup>5,8</sup> tend to find the transition at higher pressures than earlier studies on natural graphite.<sup>2,3,9</sup> The room-temperature, high-pressure post-graphite phase exhibits other interesting properties, being optically transparent<sup>4,6,8,10-12</sup> and superhard and capable of indenting diamond anvils.<sup>11</sup> In this work, we devise an experimental observable to determine the phase transition pressure at  $\sim 19 \pm 2$  GPa with little hysteresis.

Although the crystal structure of this metastable post-graphite form of carbon remains unknown, several structure measurements have been performed<sup>3,11,12</sup> and the new phase has been indexed as cubic,<sup>2,13</sup> rhombohedral,<sup>9</sup> and hexagonal.<sup>6</sup> This new structure is different from the well-studied lonsdaleite phase of carbon<sup>3</sup> as it forms at room-temperature, and, unlike the hexagonally ordered lonsdaleite, the room-temperature post-graphite phase is not quenchable to ambient pressures, except at temperatures much less than 100 K.<sup>10,12</sup> Computations have proposed multiple other structures for the post-graphite phase including metallic diamond-like K<sub>4</sub> (Refs. 14 and 15) and insulating phases: a close-packed structure of C<sub>24</sub> fullerenes,<sup>16</sup> a body-centered tetragonal allotrope named bct-C<sub>4</sub>,<sup>17</sup> and a monoclinic structure with C2/m symmetry dubbed M-carbon.<sup>18</sup>

Although there have been many electrical conductivity experiments on the high-pressure behavior of graphite, no effort has been made to observe the time-dependence of the graphite  $\rightarrow$  post-graphite transition at room temperature, i.e., the kinetics of this phase transition. We have found in our measurements that in the pressure region surrounding this phase transition, the sample resistance is highly time-dependent and reproducible and occurs during decompression and compression. Furthermore, to within our experimental precision, we find that the pressure at which the resistance changes during relaxation from increasing to decreasing and vice-versa is reversible.

## II. EXPERIMENTAL METHODS

Two measurements (referred to as Run 1 and Run 2) were taken on a single sample of highly-ordered pyrolytic

<sup>a)</sup>Electronic mail: jmontgom@uab.edu.

<sup>b)</sup>Author to whom correspondence should be addressed. Electronic mail: kanani.lee@yale.edu.

graphite. The resistance was recorded as a function of pressure and time, and samples were photographed after each adjustment of pressure. In each of these photomicrographs (Fig. 1), the gasket area was carefully mapped out and measured using VistaMetrix software (SkillCrest, LTD), and the resulting gasket area, along with the equation of state of rhenium,<sup>19</sup> was used to verify that the resistance increases measured were not due purely to geometric changes in the sample.<sup>20</sup>

To assemble the sample chamber, two strips of rhenium ribbon (0.75 mm wide  $\times$  33  $\mu$ m thick  $\times$  2 mm long) were epoxied to a flat diamond slab (3  $\times$  4  $\times$  1 mm, Sumicrystal) with a  $70 \pm 5$   $\mu$ m gap between the long axes. Copper wire was inserted into a 100  $\mu$ m glass capillary tube (for insulation from the steel diamond-anvil cell (DAC)) and attached to each gasket with conducting glue.

A square of 30  $\mu$ m-thick highly-ordered pyrolytic graphite (HOPG) was inserted into the prepared sample chamber, oriented with the graphene sheets parallel to the diamond surface to ensure compression along the *c*-axis and resistance measurement across the *a*-axis. Diamond powder was loaded around the sample to fill in the gaps between the gaskets for lateral support and to ensure continued separation of the rhenium ribbons thus preventing a short circuit. A small amount of ruby powder was used for pressure calibration.<sup>21</sup> The non-hydrostatic packing of the graphite sample and ruby powder led to pressure variations across the sample up to  $\sim$ 1-2 GPa throughout the experiment although pressure gradients across the diamond culet could have been much higher.

Resistance was measured using an AVS-45 Automatic Resistance Bridge, capable of measuring resistances within 10 m $\Omega$ . After each pressure adjustment, several measurements of pressure and resistance were taken over a long period of time until the resistance changes became either negligible or appeared to be linear with time, rather than exponentially changing. It is not clear from our measurements how long the resistance would continue to change af-

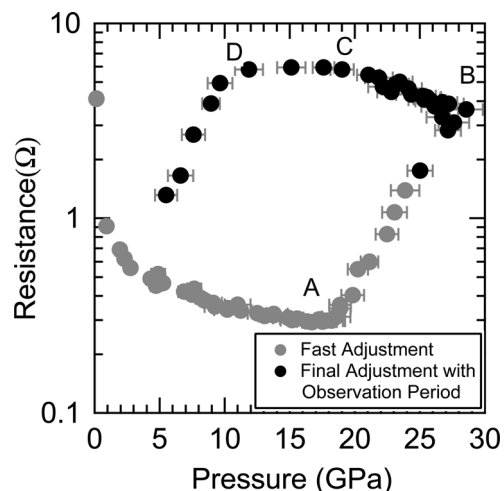


FIG. 2. Resistance versus pressure data for Run 1. Upon initial compression, the pressure was increased rapidly (gray circles), with little time ( $\sim$ 15 min) between pressure increases. The phase change was observed, indicated by the steep increase in resistance at  $\sim$ 19 GPa (point A). Near the maximum pressure of 28 GPa (point B), the resistance began to increase noticeably with time, and each change in pressure (black circles) was subsequently followed by a long observation period to detect these changes. Although the curve shows a large hysteresis in the resistance on decreasing pressure, with the return transition occurring at  $\sim$ 10 GPa (point D), it can be seen from the time-dependence of the resistance [Figs. 2-3] that the transition begins to reverse direction at point C, when the pressure was decreased back to  $\sim$ 19 GPa.

ter these points since even after exceptionally long waiting periods no deviation from linear behavior was observed. However, it is clear that the duration of this “waiting period” does affect the overall resistance vs. pressure behavior.

During Run 1, which took place over the course of 37 days, measurements were recorded manually and thus were not evenly spaced [Figs. 2-4]. During the final stages of compression and during all of the decompression stages of Run 2, resistances were recorded automatically, leading to evenly spaced measurements every 30 min [Figs. 5-7].

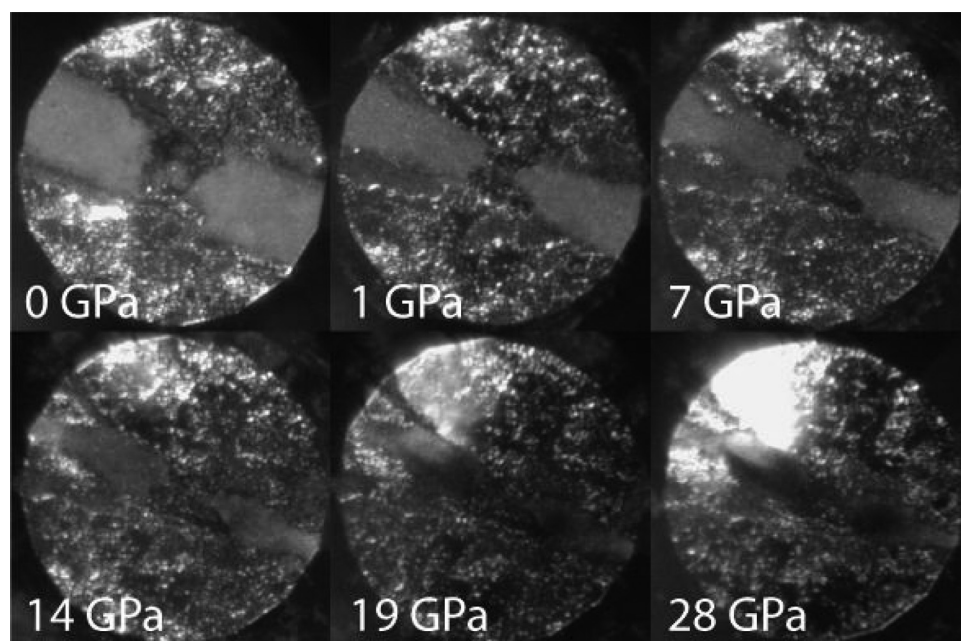


FIG. 1. Photomicrographs of the sample at various pressures during Run 1. The sample began as a 70  $\mu$ m square of HOPG remained nearly rectangular at all pressures. For reference, the diameter of the culet is 300  $\mu$ m.

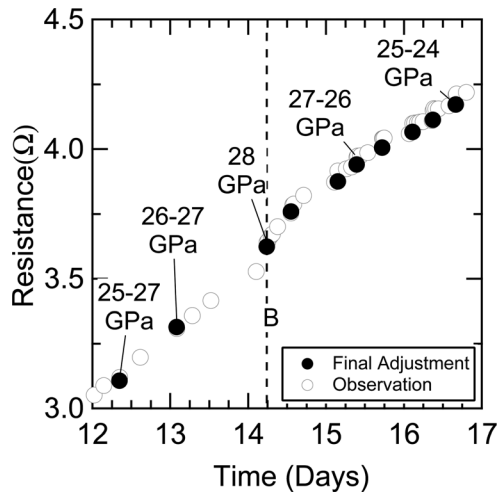


FIG. 3. Resistance versus time data for Run 1 during compression and decompression surrounding the highest compression point (point B) in Fig. 2. The open circles represent measurements made during the observation periods, while the black circles represent the measurements where the pressure was changed. Note the positive slope of the resistance versus time at high pressures on both compression (left of dashed line) and decompression (right of dashed line). Corresponding pressures are listed for reference.

Additionally, we performed resistivity calculations to investigate the overall changes in resistance between Run 1 and Run 2. Since the sample remained roughly rectangular throughout the measurement (Fig. 1), resistivity is calculated as

$$\rho = R \frac{wt}{l}.$$

Resistance is related to resistivity by a simple geometric factor consisting of the path length  $l$ , width  $w$ , and thickness  $t$ . Photomicrographs allow for the direct measurement of  $w$  and

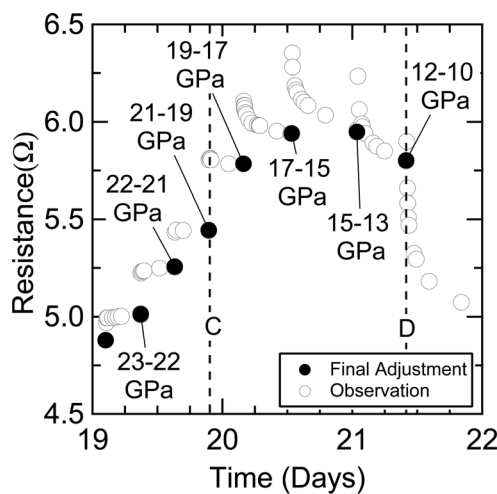


FIG. 4. Resistance versus time data for Run 1 during decompression near points C and D in Fig. 2. The open circles represent measurements made during the long observation periods, while the black circles represent the points where the pressure was changed. At point C, corresponding to the 19 GPa transition, the slope of the resistance versus time curve changes from zero to negative. At point D ( $\sim 10$  GPa), it can be seen that the decrease in resistance over time is larger than the increase seen at each adjustment, leading to an overall decrease in the resistance versus pressure behavior. Corresponding pressures are listed for reference.

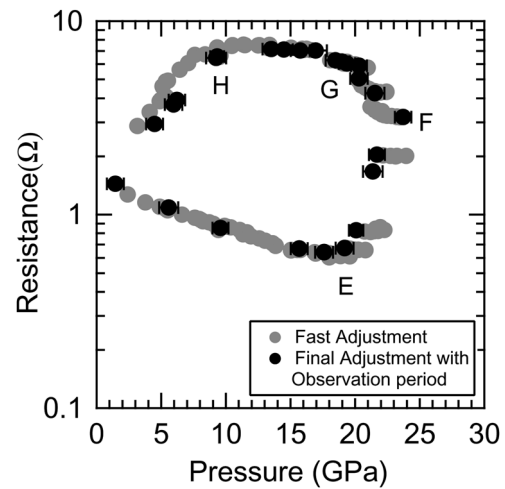


FIG. 5. Resistance versus pressure data for Run 2. Symbol notation is the same as in Fig. 2. The overall behavior was similar to that during Run 1, but several long observation periods were recorded during compression as well as decompression. Again, we observe a large resistance increase near 18-19 GPa on compression (point E), and a large hysteresis to this curve, with resistance beginning to decrease at  $\sim 9$  GPa on decompression (point H). However, we observe the change in the slope of the resistance versus time curve at points E and G [Figs. 6 and 7].

$l$ , but the thickness  $t$  of the sample is known only before and after the measurement. For all pressures other than ambient, it must be modeled.

Two models were compared for this calculation: The first model assumed a linear dependence of gasket thickness with pressure

$$t(P) = t_0 + \frac{t_f - t_0}{P_{\max} - P_0} P \approx t_0 + \frac{t_f - t_0}{P_{\max}} P,$$

where  $t_f$  and  $t_0$  are the initial and final measured thicknesses of the rhenium gasket after the experiment ( $13 \mu\text{m}$  and  $33$

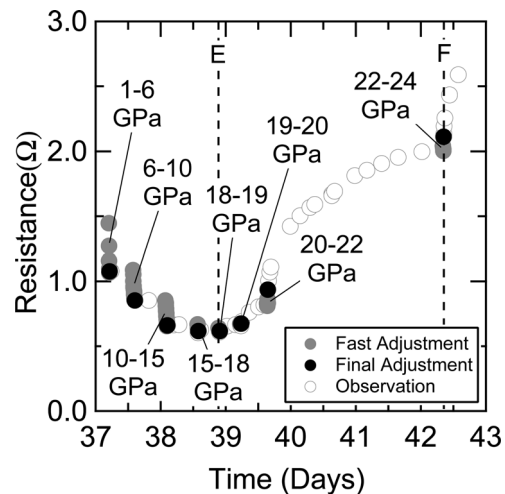


FIG. 6. Resistance versus time data for Run 2 during compression up to point F in Fig. 5. Gray and black circles represent resistance measurements taken during pressure adjustment and correspond to the respective points in Fig. 5. Open circles represent measurements taken during the long observation periods. During the loading phase of Run 2, the resistance decreased with pressure but remained constant with time up until the transition pressure (point E, 18-19 GPa) when the slope of the resistance versus time began to increase, at first slowly, and then quickly after each pressure adjustment. Corresponding pressures are listed for reference.

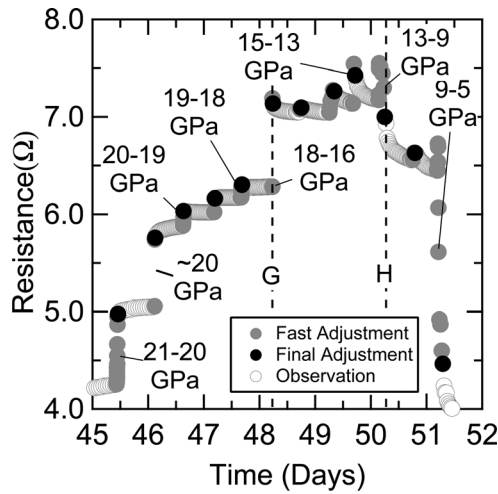


FIG. 7. Resistance versus time data for Run 2 during decompression near points G and H in Fig. 5. Symbol notation is the same as in Fig. 6. During the unloading phase of Run 2, the sample resistance exhibited nearly identical behavior to that in Fig. 4. As the transition pressure (point G, 18-16 GPa) was reached, the slope of the resistance versus pressure curve again became negative. It is possible that this transition began  $\sim 1$ -2 GPa earlier, where the slope becomes flat. At point H, these resistance drops became larger than the increase seen at each adjustment, and thus the resistance drops become apparent in the overall resistance versus pressure behavior. Corresponding pressures are listed for reference.

$\mu\text{m}$ , respectively) and  $P_0$  and  $P_{\text{max}}$  are atmospheric pressure and the maximum pressure reached of 28 GPa.

The second model relied on an assumption that the amount of rhenium gasket material flowing out from the culet edges was proportional to the amount of rhenium flowing inward. Volume changes in rhenium due to pressurization were taken into account. The thickness of the gasket in this model is given by

$$t(P) = \frac{v(P)A_{R0}t_0}{(1+n)A_R(P) - nA_{R0}},$$

where  $v(P)$  is the fractional change in the rhenium volume due to applied pressure,  $A_{R0}$  is the initial measured gasket area under the culet,  $A_R$  is the measured area of the gasket, and  $n$  a parameter relating the amount of rhenium that is squeezed outside of the culet to that which is squeezed inwards. The parameter  $n$  is found from the initial and final gasket thicknesses and the gasket areas measured at the lowest and highest pressures

$$n = \frac{v(P_f)A_{R0}t_0 - A_R(P_f)t_f}{(A_R(P_f) - A_{R0})t_f}.$$

Both thickness models and calculated errors are plotted in Fig. 8, and the associated geometric factor for each is shown in Fig. 9.

### III. THEORETICAL METHODS

To complement our resistance measurements, we used density-functional theory (DFT) to investigate the electronic density of states for graphite, lonsdaleite, diamond, bct-C<sub>4</sub>, and M-carbon at pressures of 0, 15, and 25 GPa [Fig. 10].

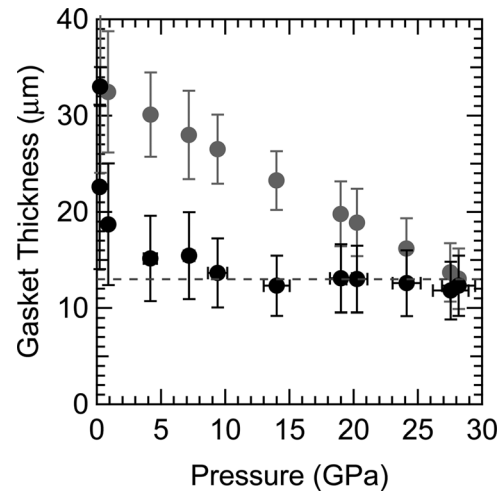


FIG. 8. Two models of gasket thickness used for resistivity calculations for measurements taken during the initial compression (Run 1). Gray symbols correspond to a model where gasket thickness changes linearly with pressure, while black symbols correspond to a model where gasket material is allowed to flow out between the culet edges and to compress with applied pressure.

Interactions between carbon nuclei were described within the projector-augmented wave (PAW) formalism<sup>22</sup> with electron configuration  $[\text{He}]2s^22p^2$  and core radius of 1.500 a.u., as implemented in the Vienna *ab-initio* simulation package (VASP).<sup>23</sup> Electronic exchange and correlation effects were described within the Perdew-Burke-Ernzerhof (PBE) functional.<sup>24</sup> The plane-wave cutoff energy in all calculations was  $E_{\text{cut}} = 800$  eV and  $\Gamma$ -centered  $9 \times 9 \times 5$ ,  $9 \times 9 \times 5$ ,  $6 \times 6 \times 6$ ,  $5 \times 5 \times 9$ , and  $3 \times 9 \times 5$  k-point grids, for graphite, lonsdaleite, diamond, bct-C<sub>4</sub>, and M-carbon, respectively. All symmetry-allowed geometrical degrees of freedom were relaxed, and the electronic density of states (eDOS) were calculated for the relaxed structures. These computational

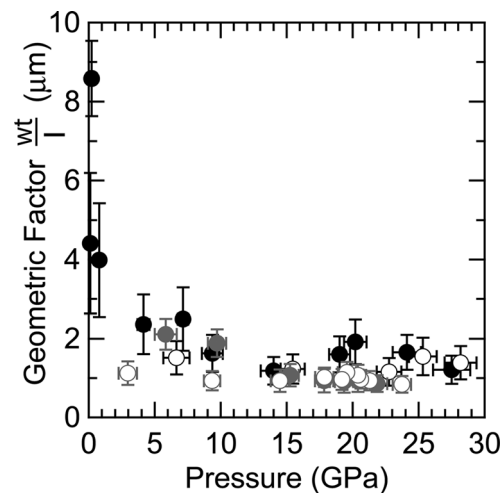


FIG. 9. Geometric factor  $wt/l$  in the resistivity calculation as calculated from the gasket-flow model for Run 1 (black symbols) and Run 2 (gray symbols). Filled symbols represent compression, while open symbols represent decompression. It can be seen that this factor is approximately the same at all pressures for both Run 1 and Run 2 and thus cannot be a factor in the overall change in resistance.

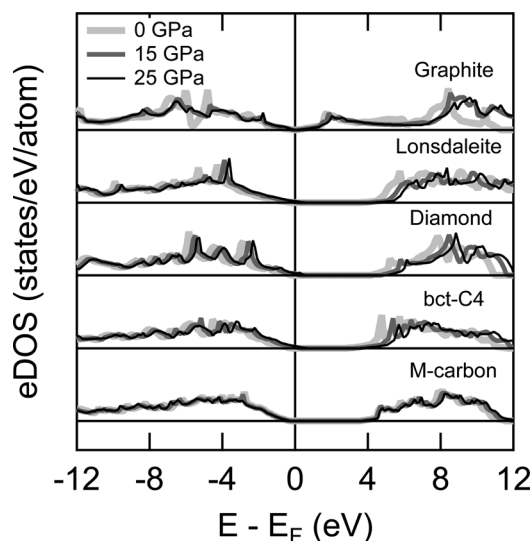


FIG. 10. The total eDOS as computed by GGA for graphite, lonsdaleite, diamond, bct-C<sub>4</sub>, and M-carbon at 0 GPa (light gray), 15 GPa (dark gray), and 25 GPa (black). All phases of carbon except for graphite show a large band gap, yielding insulating behavior as compared to semimetallic graphite. The eDOS of all phases show little variation with pressure at least up to 25 GPa.

settings are similar to previous computational work on carbon structures.<sup>17,18,25</sup>

#### IV. RESULTS AND DISCUSSION

In Run 1, the pressure was increased quickly (over the course of a few hours) until the resistance increase (A) indicated a transition [Fig. 2]. Up until this point, no significant time dependence of the sample resistance was observed. This observation is consistent with the expectation that the pressure-induced adjustments of the electronic structure are fast as compared to structural changes. However, at  $P > \sim 19$  GPa the resistance did not stabilize for several hours [Fig. 3]. The large (between 0.1 and 0.5  $\Omega$ ) resistance increases observed immediately after each pressure adjustment [e.g., Fig. 4, solid circles] are caused by instantaneous resistance changes to the sample resulting from the pressure adjustment. In an effort to quantify these changes, the sample resistance was recorded for an extended period of time between pressure adjustments, and it was observed that the resistance increased with time [Fig. 3]. This observation is consistent with a sluggish phase transition to an insulating high-pressure phase. This behavior continued up until the maximum pressure attained in this study ( $\sim 28$  GPa). The resistance continued to increase with time during the initial decompression stages. However, the rate was significantly lower as compared to compression, consistent with a continued but decreasing driving force for the formation of the high-pressure phase as the pressure is lowered toward the phase transition pressure that was observed in this study during compression,  $P_{tr} \sim 19$  GPa. However, beginning at  $P_{tr}$  during decompression [Fig. 4, point C], the resistance stopped increasing, and by 17 GPa it began to drop with time. By 10 GPa [Fig. 4, point D], the resistance decrease seen during the observation period was greater than the increase due to pressure adjustment (i.e., greater than the 0.1 and 0.5  $\Omega$  change observed due to

physically manipulating the DAC when changing the pressure), and it is at this point that the decrease can be seen in the resistance versus pressure behavior [Fig. 2].

Upon completion of Run 1, the sample was re-compressed in Run 2: the pressure was increased by  $\sim 5$  GPa below the transition and in  $\sim 1$ -2 GPa steps near and above the transition. During compression, the resistance showed no change (within the experimental error of 0.01  $\Omega$ ) with time up until 19 GPa [Figs. 5 and 6, point E]. At that point, the resistance began to increase with time and continued to do so up through the maximum pressure of  $\sim 24$  GPa [Figs. 5 and 6, point F] and during decompression, until  $\sim 20$  GPa, when the slope became zero within the experimental error [Fig. 7]. At  $\sim 18$  GPa [Fig. 7, point G], the resistance began to decrease with time, and by 10 GPa [Fig. 7, point H] these resistance drops were larger than the resistance increases seen at each pressure adjustment, and it is here that the decrease in resistance becomes apparent in Fig. 5, consistent with observations in Run 1 [Fig. 2].

*In situ* microphotographs fail to confirm or deny this post-graphite phase as optically transparent as observed in past studies,<sup>4,6,8,10-12</sup> likely due to the large sample thicknesses ranging between 13–33  $\mu\text{m}$  [Fig. 1]. However, parts of the sample chamber became transparent upon pressure and reverted back to opaque upon decompression, indicating that the high-pressure phase is semiconducting or insulating.

The resistivity calculations performed suggest that the overall increase in resistance after Run 1 is due to inherent resistivity increase in the sample and is not due to any geometric changes between the two runs (Figs. 8 and 9). This increase in resistance is likely due to a loss of the “highly-ordered” nature of the HOPG sample. The initial decrease of the resistance of graphite under pressure is expected as the eDOS at the Fermi level increases with increasing pressure<sup>7</sup> [Fig. 10]. Lonsdaleite, diamond, bct-C<sub>4</sub>, and M-carbon<sup>18</sup> are electronic insulators and the eDOS, and in particular the band gap is predicted to depend weakly on pressure, at least up to 25 GPa [Fig. 10]. The rapid change of the pressure dependence of the resistance at  $P \sim 19$  GPa is consistent with kinetically hindered  $sp^2 \rightarrow sp^3$  re-hybridization across the phase transition. Thus, the observed time dependence of resistance during relaxation is likely related to the sluggish conversion of graphite to the high-pressure post-graphite phase.

The slope of the resistance versus time graphs [Figs. 3, 4, 6, and 7] can be used to accurately identify the transition pressure in graphite occurring at 19 ( $\pm 2$ ) GPa. This result conflicts with previous resistance measurements that show a large  $\sim 10$  GPa hysteresis of graphite but is consistent if the rate of structural change is proportional to pressure as would be expected for a kinetically hindered phase transition. Furthermore, from the Run 2 data during decompression [Fig. 7] it can be seen that there is a pressure range (2-3 GPa) in which the slope of the resistance versus time curve remains zero, possibly indicating that there may be a small residual hysteresis which could be removed if the relaxation would be tracked for even longer times or this may be due to the non-hydrostaticity in the sample.

The discrepancies between our determination of this transition pressure and those of previous electrical resistance

measurements and x-ray diffraction,<sup>1–5</sup> which themselves do not agree, may depend on the experimental geometry and hydrostaticity of the measurement techniques and/or on the highly ordered nature of the graphite sample used. However, the observed hysteresis in resistance is explainable as an artifact of the time-dependence of the sample resistivity. The rate of decrease of the resistance with time was large enough in both Runs that the time each sample was allowed to relax at low pressures influenced the observed drop-off in resistance with pressure. Since Run 1 was left at lower pressures for longer times, the resistance drops more with pressure than Run 2 [Figs. 2 and 5]. Given a sufficiently long enough “observation period” between pressure changes, it is likely that the observed residual hysteresis would vanish, leading to a thermodynamically well-defined transition pressure as expected for a one-component system.

## V. CONCLUSIONS

We have observed the room-temperature post-graphite phase transition and established that the resistance of graphite has a large time-dependent component near the transition pressure. Below the transition pressure the resistance decreases with time during relaxation, while above this pressure the resistance increases with time, consistent with our and other theoretical predictions that the post-graphite phases should be semiconducting or insulating<sup>16–18,25</sup> [Fig. 10]. These results also indicate that instantaneous resistance changes are insufficient to precisely determine the transition pressure, at least in the case of carbon. This situation can be significantly improved by observing resistance changes during relaxation across the phase transition, thus allowing an accurate determination of the true phase boundary. The time dependence also largely removes the uncertainty of the pressure of the transition, which is now recognized to be an artifact of the sluggishness of this graphite to post-graphite transition. Although these resistance measurements do not allow discrimination between proposed post-graphite phase, such as M-carbon and bct-C<sub>4</sub>, the results suggest that patience is likely necessary to fully appreciate the complex-

ity of the potential energy surface of elemental carbon and the selectivity toward crystal structures other than diamond. We also show that time-dependent relaxation, at least in the case of carbon, has to be an integral part of re-establishing consistency between commonly used exploration techniques for materials behavior at high pressures.

## ACKNOWLEDGEMENTS

We thank Stefanie Japel and Heinz Nakotte for experimental help, Yuejian Wang for discussions, and RV Elektronika for technical assistance.

- <sup>1</sup>G. A. Samara and H. G. Drickamer, *J. Chem. Phys.* **37**, 471 (1962).
- <sup>2</sup>R. B. Aust and H. G. Drickamer, *Science* **140**, 817 (1963).
- <sup>3</sup>F. P. Bundy and J. S. Kasper, *J. Chem. Phys.* **46**, 3437 (1967).
- <sup>4</sup>X. Y. Li and H. K. Mao, *Phys. Chem. Miner.* **21**, 1 (1994).
- <sup>5</sup>N. Okuyama, H. Yasunaga, and S. Minomura, *Jpn. J. Appl. Phys.* **10**, 1645 (1971).
- <sup>6</sup>T. Yagi, W. Utsumi, M. A. Yamakata, T. Kikegawa, and O. Shimomura, *Phys. Rev. B* **46**, 6031 (1992).
- <sup>7</sup>J. R. Patterson, S. A. Catledge, and Y. K. Vohra, *Appl. Phys. Lett.* **77**, 851 (2000).
- <sup>8</sup>W. Utsumi and T. Yagi, *Science* **252**, 1542 (1991).
- <sup>9</sup>Y. X. Zhao and I. L. Spain, *Phys. Rev. B* **40**, 993 LP (1989).
- <sup>10</sup>J. V. Badding and A. D. Lueking, *Phase Trans.* **80**, 1033 (2007).
- <sup>11</sup>W. L. Mao, H. K. Mao, P. J. Eng, T. P. Trainor, M. Newville, C. C. Kao, D. L. Heinz, J. F. Shu, Y. Meng, and R. J. Hemley, *Science* **302**, 425 (2003).
- <sup>12</sup>E. D. Miller, D. C. Nesting, and J. V. Badding, *Chem. Mater.* **9**, 18 (1997).
- <sup>13</sup>R. W. Lynch and H. G. Drickamer, *J. Chem. Phys.* **44**, 181 (1966).
- <sup>14</sup>T. Sunada, *Notice AMS* **55**, 208 (2008).
- <sup>15</sup>M. Itoh, M. Kotani, H. Naito, T. Sunada, Y. Kawazoe, and T. Adschiri, *Phys. Rev. Lett.* **102**, 055703 (2009).
- <sup>16</sup>V. V. Pokropivny and A. V. Pokropivny, *Phys. Solid State* **46**, 392 (2004).
- <sup>17</sup>K. Umamoto, R. M. Wentzcovitch, S. Saito, and T. Miyake, *Phys. Rev. Lett.* **104**, 125504 (2010).
- <sup>18</sup>Q. Li, Y. M. Ma, A. R. Oganov, H. B. Wang, H. Wang, Y. Xu, T. Cui, H. K. Mao, and G. T. Zou, *Phys. Rev. Lett.* **102**, 175506 (2009).
- <sup>19</sup>R. Jeanloz, B. K. Godwal, and C. Meade, *Nature* **349**, 687 (1991).
- <sup>20</sup>J. Montgomery, M.S. thesis, New Mexico State University, 2008.
- <sup>21</sup>H. K. Mao, J. Xu, and P. M. Bell, *J. Geophys. Res.* **91**, 4673 (1986).
- <sup>22</sup>G. Kresse and D. Joubert, *Phys. Rev. B* **59**, 1758 (1999).
- <sup>23</sup>G. Kresse and J. Furthmuller, *Phys. Rev. B* **54**, 11169 (1996).
- <sup>24</sup>J. P. Perdew, K. Burke, and M. Ernzerhof, *Phys. Rev. Lett.* **77**, 3865 (1996).
- <sup>25</sup>Y. Liang, W. Zhang, and L. Chen, *Europhys. Lett.* **87**, 56003 (2009).